Multi-shot Calibration Technique for Microwave Imaging Systems

Multi-shot Calibration Technique for Microwave Imaging Systems

David O. Rodriguez-Duarte
Dept. Electr. and Telecommunications
Politecnico di Torino,
Torino, Italy
Email:david.rodriguez@polito.it

Jorge A. Tobon Vasquez
Dept. Electr. and Telecommunications
Politecnico di Torino,
Torino, Italy
Email:jorge.tobon@polito.it

Francesca Vipiana
Dept. Electr. and Telecommunications
Politecnico di Torino,
Torino, Italy
Email:francesca.vipiana@polito.it

***Abstract*—This paper proposes a novel "multi-shot" calibration technique that reduces imaging microwave reconstructions artifacts, compensating for uncontrolled variations during the measuring process and later propagated in the inversion. The calibration combines different consecutive sets of measured data with simulated ones in a post-processing stage, providing benefits without the need for additional experimental reference calibrations. The proposed scheme is tested experimentally in a non-trivial scenario. A microwave scanner images an early-stage hemorrhagic stroke in the left parietal lobe, applying a differential imaging algorithm based on the truncated singular value decomposition. Though, the proposed mechanisms can be used for other microwave imaging devices. The results reveal that the calibration procedure improves the quality of the retrieved images compared to the non-calibrated approach, cleaning the images and making the interpretation of imaged contrast variation easier.**

***Index Terms*—Measurements calibration, microwave imaging, numerical simulation, microwave antenna arrays, microwave propagation.**

I. Introduction

Microwave imaging (MWI) is a technology that relies on the contrast of the electrical properties (permittivity and conductivity) at microwave frequencies between a target and its background to retrieve quantitative or qualitative images of a domain of interest (DOI). Therefore, quantitative algorithms as the distorted Born iterative method (DBIM) or the contrast source inversion (CSI) algorithm aim to recover the actual dielectric values [1], [2]. In contrast, qualitative ones focus on identifying the location and shape of the contrast, e.g., the truncated singular value decomposition (TSVD) applied to weak scatters [3]. MWI approaches thus a nonlinear and ill-posed inverse scattering problem moving from a limited number of measurements, usually out of DOI, to a description of dielectric map in DOI [4]. Hence, a non-well-conditioned problem and corrupted input data might cause unwanted artifacts on the retrieved images.

MWI is a technology with a high potential of applicability on day-to-day problems due to its characteristics of penetrability and non-ionizing nature that have allowed it to spread over several fields. For instance, it is being researched in medical applications where pathological conditions present traceable variations in time as breast cancer [5], brain stroke [6], [7], cervical diseases [8], knee injuries [9]. Moreover, MWI has been used in the industrial domain for food quality assessment [10]–[12]. As a solution, MWI is projected as a complement to other imaging alternatives most of the time, e.g., ultrasound or magnetic resonant imaging (MRI). MWI is a technology in development and thus faces multiple challenges, especially in the applied field.

In all real scenarios, the MWI systems deal with weak signals, highly affected by the noise, suffering the introduction of different types of errors and variations compared to the ideal nominal contexts. Thus, calibration techniques are required to mitigate these unavoidable issues. For example, it is common practice in our days to use preliminary know-scenarios or targets to tune or characterize the MWI device [5]–[7], [13], [14]. Also, it can be applied novel techniques like the one proposed by the authors in [15], where instead of rendering the measurement close to the EM operator, it is calibrated using the measured and simullated data. Another novel approach, yet application depending, is presented in [11], where the authors propose a phaseless parametric inversion for system calibration. In general, the calibration aims to reduce the undesired perturbation's effects on the final dielectric mapping applying diverse strategies.

Here, we propose a novel "multi-shot" calibration technique that reduces imaging microwave reconstructions artifacts, compensating for uncontrolled variations during the measuring process as shown later in Sect. IV. The calibration combines different consecutive sets of measured data with simulated ones in post-processing, extrapolating the information of interest. Thus, the technique provides a good trade-off between the data required and benefits on the imaging reconstruction. It just needs an additional set of measurements, which is a reasonable condition for many systems. Moreover, the proposal is a complementary alternative to other calibration solutions, easily implementable since no additional hardware or complex setups are required.

The paper is organized as follows. Section II comments on the MWI prototype, the imaging algorithm, as well as describes the "multi-shot" calibration procedures. Section Sect. III details the experimental validation including the setup and results. Finally, Sect. V presents the conclusions and future work.

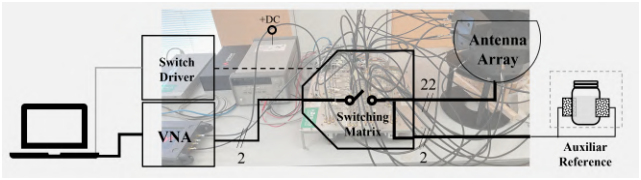

Fig. 1. Schematic description of the multi-shot procedure

II. Methods

A. MWI Prototype

Generally, an MWI system consists of an array of antennas surrounding the DOI while acting as transmitters and receivers. The antennas then sample the total and incident fields, from which the imaging algorithm recovers the scattered field in the DOI. In the specific case of this work, for the experimental validation, we use the system presented in [6], [16].

The system consists of 24 brick-shaped antennas that work around 1 GHz. Each antenna is a printed monopole immersed in brick of matching that improves the coupling of the impinged signals [17]. The second component is the Vector Network Analyzer (VNA). It generates the stimulus signals injected into DOI, while measures the reflection and transmission. Here, we use a compact 2-port P9375A Keysight Streamline USB VNA [18]. Then, to move from the 2-port for VNA to the 24-antenna ones, we use a switching matrix that employs electromechanical coaxial switches [19]. We connect each antenna to its respective switch via a flexible coaxial cable. Figure 1 depicts an overview of the system.

Moreover, two antennas are reserved as auxiliary reference for calibration. These are placed in the vicinity of a reference phantom, filled with a liquid mimicking the electric properties of the average brain. Further details on the system and the reference channel are in [6].

B. Imaging Algorithm

Here we use a qualitative descriptive imaging algorithm for approach an stroke pathology as in [6], [16]. The algorithm employs a differential scheme receiving as input the differential scattering matrix regarding two different instants. It also required a nominal electric field, generally obtained via full-wave simulation of a virtual twin [16], [20]. Therefore, the algorithm aims to recover the variation between the times t_0 and t_1 of the dielectric contrast on DOI, defined as

$$\Delta\chi(t_0, t_1) = \frac{\epsilon(t_1) - \epsilon(t_0)}{\epsilon_b}, \tag{1}$$

where $\epsilon(t_0)$ and $\epsilon(t_1)$ are the complex permittivities, and b stands for the background scenario. Then $\Delta\chi$ contrast is linked to the measured differential scattering matrix ΔS at t_0 and t_1, via the radiated electric fields in DOI by the antenna in p at t_0 and by the antenna in q at t_1 ($\mathbf{E}_p(t_0)$ and $\mathbf{E}_q(t_1)$) as

$$\Delta S(t_0, t_1) = -\frac{j\,\omega\,\epsilon_b}{2\,a_p\,a_q} \int_{DOI} \mathbf{E}_p(t_0) \cdot \mathbf{E}_q(t_1)\,\Delta\chi\,d\mathbf{r}, \tag{2}$$

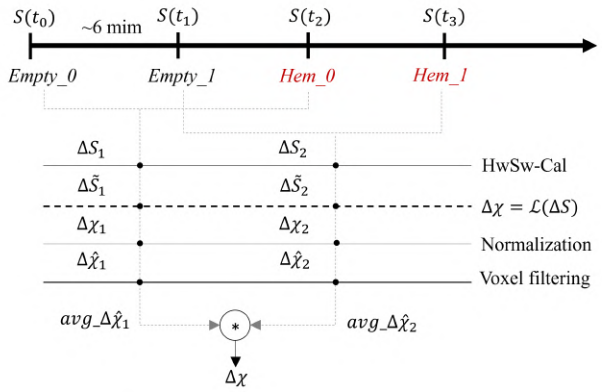

Fig. 2. Schematic description of the multi-shot procedure

where the symbol "·" denotes the dot product between vectors, j is the imaginary unit, $\omega = 2\pi f$ is the angular frequency, and a_p and a_q are the known incoming root-power waves at the p and q antenna ports, respectively [21]. Hence, applying the the Born approximation, reasonable approach in monitoring concentrate variation, the electric field radiated at t_1 is equaled to the initial one radiated at t_0, linearizing (2). Then, the unknown dielectric contrast can be obtained using the truncated singular value decomposition (TSVD) scheme as

$$\Delta\chi = \sum_{n=1}^{T} \frac{1}{\sigma_n} \langle \Delta S, u_n \rangle\, v_n, \tag{3}$$

where $\langle u, \sigma, v \rangle$ is the SVD of the discretized scattering operator $\mathcal{S}$ and T is the truncation index that acts as a regularization parameter [3].

C. Calibration Procedure

The diagram in Fig. 2 describes the general scheme of the calibration and the data flow, evidencing the need for at least four sets of measurements in the case of a differential imaging approach, two for each studied state, to arrive at a single image. Here, we consider as the first state, the healthy(empty), and the second one the Hemorrhage (Hem). Thus, the calibration assumes that the variation of the scenario in a state, i.e., between each set of two consecutive measures, is almost null or very mild compared to the variation between states. This constrain is determined in real applied problems by the measured time and the speed of the variation of the studied scenario.

Then, if the input data meets the conditions, a four-step procedure is applied to each differential pair to finally perform and average of the two retrieved contrast. The final averaging acts similarly to the MUSIC algorithm [22], but here instead of overlapping between frequency responses, it used the response to different reconstructions of the same scenario, at close-by instant, at the same frequency. Also, it bears similarities to traditional averaging used by VNAs to improve their Signal-to-noise-ratio (SNR) [23]. Still, in this case, it is considered the noise propagation on the imaging algorithm.

Considering the left branch, as the other is equivalent, the first step is to apply the dubbed "HwSw-Cal", which uses hardware and software calibration [6]. The hardware part (HW) bases on the transmission coefficients measured in the auxiliary reference channel described in Sect. II-A, and aims to reduce the effects of multiplicative inaccuracies on scattering transfer parameters between all the antenna pairs. For instance, HW calibration faces drift errors in the VNA and/or in the switching matrix and uncertainties due to environmental conditions.The HW calibration used the S-parameters of the channel at t_0 and t_1, which is not affected by the intentional variation in DOI, to compensate the response at t_1 as shown in Eq. 4. A more detailed explanation of the Hw calibration can be seen in [6].

$$\overline{\Delta S}_{p,q}(t_0,t_1) \quad = \quad S_{p,q}(t_0) - \frac{S^{\mathrm{REF}}(t_0)}{S^{\mathrm{REF}}(t_1)} S_{p,q}(t_1) \quad (4)$$

In addition to the described Hw calibration, a second calibration, "software calibration" (Sw), is also applied. This technique uses a known scenario in both the numerical modeling and the real system [13]. Then to adjust the measurements, we apply the HW calibrated data to the SW calibration as write in Eq. 5, which has shown reach better results than just applied one of them [6].

$$\widetilde{\overline{\Delta S}}_{p,q}(t_0,t_1) = \frac{\tilde{S}^{\mathrm{H}}_{p,q}}{S^{\mathrm{H}}_{p,q}} \overline{\Delta S}_{p,q}(t_0,t_1), \quad (5)$$

where $\tilde{S}^{\mathrm{H}}_{p,q}$ and $S^{\mathrm{H}}_{p,q}$ are the simulated and measured scattering parameters for the generic p,q antenna pair in the known case, respectively. Here, we use healthy state as known scenario.

Once the scattering parameters are calibrated, the retrieved dielectic maps are obtained projecting the calibrated differential scattering data into the linearized operator (see Sect. II-B). Then, the contrasts are normalized and interpolated in a 1 mm^3 voxel grid, tetrahedral one initially, to later apply a voxel filtering. The voxel filter acts as a low-pass filter on the data, removing the spikes(atypical points) on the reconstructions and smoothing the image. It performs a 3-D average as illustrated in Fig. 3, where the voxel in blue is averaged with its neighbors. Thus, depending on the voxel's position in DOI, it enters in one of the depicted cases. Though, most of the voxels consider its 29 closest surrounding neighbors. Figure 4 presents a comparison between a filtered and non-filtered case.

Finally, after getting the two pre-proceced contrast maps, a point to point averaging between them is applied. Here, it is worth noticing that the averaging might be further extended using the cases $S(t_3) - S(t_0)$ and $S(t_2) - S(t_1)$.

III. Experimental Validation

For the experimental validation, we set a simplified monitoring scenario of an early-stage stroke using a 3-D printed single cavity anthropomorphic head phantom [24], and plastic pod for mimic the stroke as shown in Fig. 5. These are filled with mixtures mimicking the electrical properties of the average brain tissues and blood, around $\epsilon_r = 45, \sigma = 0.7$ and $\epsilon_r = 65, \sigma = 1.55$ at 1 GHz, respectively [6]. Moreover, the stroke dimension and its location were based on a left parietal lobe lesion, pathology that might cause speech impairments [25]. This modeled situation is specially challenging considering the dimensions and non-even shape of the stroke target as shown in Fig. 5.

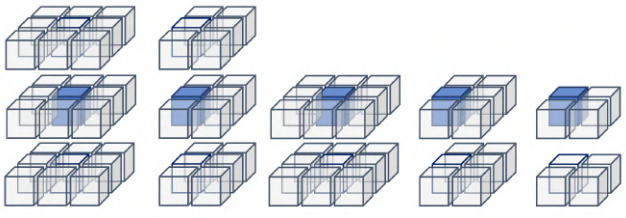

Fig. 3. Volxel filtering considering the different vicinity configurations. The blue voxel indicates the filted one.

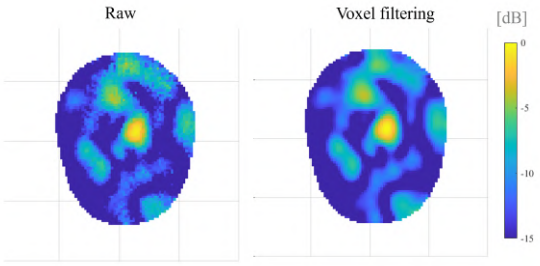

Fig. 4. Reconstruction applying and without applied voxel filtering.

The validation then considers two sets of consecutive measures (shot) of the healthy (without the stroke) and unhealthy situations, i.e., two initial measures of the healthy scenario and then two unhealthy ones. Though, this configuration might also represent the variation between to different states of an stroke. The VNA is set measures around 1 GHz, with input power of -6 dBm and the intermediate filter (IF) to 50 Hz, reaching a the noise floor above -110 dB. The measuring time of the whole 24×24 S-matrix is in the order of the 6 minutes per set, however, there is an additional time slot between the healthy an unhealthy measurements, that was used to introduce the stroke inside the head. Besides, for the unhealthy cases, the stroke is fixed in its position using a wooden stick and an external support.

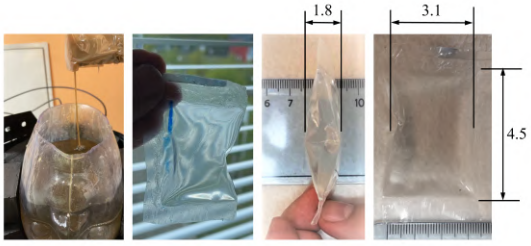

Fig. 5. Phantoms used during the experiment. (Left-to-right):Anthropomorphic head phantom with target hold inside; pod-shaped stroke; lateral view; frontal view. All dimensions in [cm].

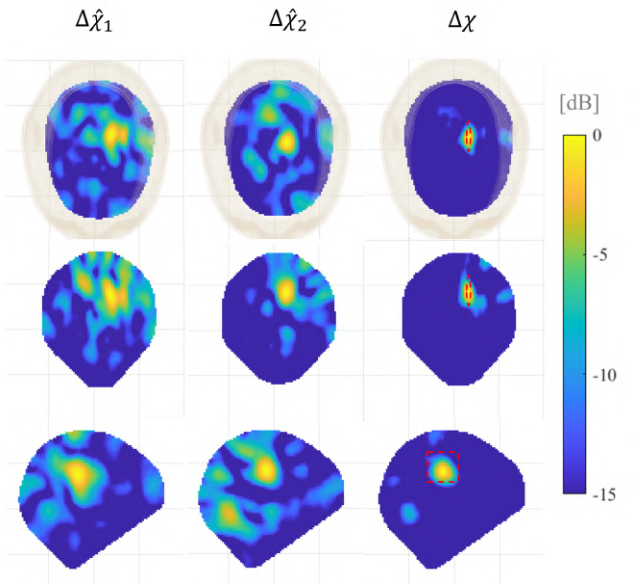

Fig. 6. Amplitude normalized of the reconstructed dielectric contrast. (Top-to-bottom Rows):Transverse plane; Frontal plane; Saggital plane. The red squares in the right column indicates the position and shape of the stroke.

IV. Results

The results are summarized in Fig. 6. The columns refer to the normalized reconstructed dielectric contrast using the different sets of differential S-parameters, healthy and unhealthy scenarios, and the one applying the "multi-shot" calibration. The rows consider the transverse, frontal, and sagittal planes center at the maximum of each reconstruction. Here, it is worth mentioning that the resulting contrast is a 3-D image, although just the main views are presented.

From the results, it can be noticed first that the imaging algorithm can identify the location of the stroke correctly and with a reasonable estimation of the shape in all cases. Also, it is noticeable from the non-multi-shot calibrated results the repetitively of the experiment, yet the artifacts generated by the remained non-HwSw-calibrated disturbances.

On the other hand, The calibrated results improve the quality of the retrieved images, removing a large number of artifacts. The final results show a precise detection of the stroke, isolated from the background, and a good shape retrieval even in the shortest dimension of the target (less than 2 cm).

V. Conclusions

This work presented an off-line complementary calibration tool that allows improving the quality of the reconstruction from a microwave imaging system using a "multi-shot" approach. The proposed technique counterbalances the undesired perturbation propagated in the imaging using a double set of measurements and reconstructions. Here, the technique was applied to imaging a brain stroke, experimentally emulated, showing significant improvements on the resulting images. Though, the technique could be used as complementary calibration for other MWI systems. We aim to extend the validation of the "multi-shot" calibration testing in complex scenarios and other MWI systems for future work.

Acknowledgment

The authors would like to acknowledge the valuable help of Eng. Gianluca Dassano for the realization of the switching matrix. Moreover, the anthropomorphic 3-D printed plastic head container was provided by Prof. Nadine Joachimowicz and Prof. Bernard Duchêne. This work was funded by the Italian Ministry of University and Research under the PRIN project "MiBraScan—Microwave Brain Scanner for Cerebrovascular Diseases Monitoring", and by the European Union's Horizon 2020 research and innovation program under the EMERALD project, Marie Skłodowska-Curie grant agreement No. 764479.

References

[1] A. Zakaria, C. Gilmore, and J. LoVetri, "Finite-element contrast source inversion method for microwave imaging," *Inverse Problems*, vol. 26, p. 115010, sep 2010.

[2] Z. Miao and P. Kosmas, "Multiple-frequency dbim-twist algorithm for microwave breast imaging," *IEEE Transactions on Antennas and Propagation*, vol. 65, no. 5, pp. 2507–2516, 2017.

[3] M. Bertero and P. Boccacci, *Introduction to inverse problems in imaging*. CRC press, 2020.

[4] B. J. Mohammed, A. M. Abbosh, S. Mustafa, and D. Ireland, "Microwave system for head imaging," *IEEE Transactions on Instrumentation and Measurement*, vol. 63, no. 1, pp. 117–123, 2014.

[5] D. M. Godinho, J. Felicio, C. A. Fernandes, and R. C. Conceicao, "Experimental evaluation of an axillary microwave imaging system to aid breast cancer staging," *IEEE Journal of Electromagnetics, RF and Microwaves in Medicine and Biology*, pp. 1–1, 2021.

[6] D. O. Rodriguez-Duarte, J. A. Tobon Vasquez, R. Scapaticci, G. Turvani, M. Cavagnaro, M. R. Casu, L. Crocco, and F. Vipiana, "Experimental validation of a microwave system for brain stroke 3-d imaging," *Diagnostics*, vol. 11, no. 7, 2021.

[7] A. S. M. Alqadami, A. Zamani, A. Trakic, and A. Abbosh, "Flexible electromagnetic cap for three-dimensional electromagnetic head imaging," *IEEE Transactions on Biomedical Engineering*, vol. 68, no. 9, pp. 2880–2891, 2021.

[8] C. Dachena, A. Fedeli, A. Fanti, M. B. Lodi, M. Pastorino, and A. Randazzo, "Microwave imaging for the diagnosis of cervical diseases: A feasibility analysis," *IEEE Journal of Electromagnetics, RF and Microwaves in Medicine and Biology*, vol. 5, no. 3, pp. 277–285, 2021.

[9] K. S. Sultan, B. Mohammed, M. Manoufali, and A. M. Abbosh, "Portable electromagnetic knee imaging system," *IEEE Transactions on Antennas and Propagation*, vol. 69, no. 10, pp. 6824–6837, 2021.

[10] J. A. Tobon Vasquez, R. Scapaticci, G. Turvani, M. Ricci, L. Farina, A. Litman, M. R. Casu, L. Crocco, and F. Vipiana, "Noninvasive inline food inspection via microwave imaging technology: An application example in the food industry," *IEEE Antennas and Propagation Magazine*, vol. 62, no. 5, pp. 18–32, 2020.

[11] C. Gilmore, I. Jeffrey, M. Asefi, N. T. Geddert, K. G. Brown, and J. Lovetri, "Phaseless parametric inversion for system calibration and obtaining prior information," *IEEE Access*, vol. 7, pp. 128735–128745, 2019.

[12] M. Ricci, B. Štitić, L. Urbinati, G. D. Guglielmo, J. A. T. Vasquez, L. P. Carloni, F. Vipiana, and M. R. Casu, "Machine-learning-based microwave sensing: A case study for the food industry," *IEEE Journal on Emerging and Selected Topics in Circuits and Systems*, vol. 11, no. 3, pp. 503–514, 2021.

[13] C. Gilmore, P. Mojabi, A. Zakaria, M. Ostadrahimi, C. Kaye, S. Noghanian, L. Shafai, S. Pistorius, and J. LoVetri, "A wideband microwave tomography system with a novel frequency selection procedure," *IEEE Transactions on Biomedical Engineering*, vol. 57, no. 4, pp. 894–904, 2010.

[14] B. Sohani, J. Puttock, B. Khalesi, N. Ghavami, M. Ghavami, S. Dudley, and G. Tiberi, "Developing artefact removal algorithms to process data from a microwave imaging device for haemorrhagic stroke detection," *Sensors*, vol. 20, no. 19, 2020.

[15] D. O. Rodriguez-Duarte, J. A. Tobon Vasquez, and F. Vipiana, "Hybrid simulation-measurement calibration technique for microwave imaging systems," in *2021 15th European Conference on Antennas and Propagation (EuCAP)*, pp. 1–5, 2021.

[16] J. A. Tobon Vasquez, R. Scapaticci, G. Turvani, G. Bellizzi, D. O. Rodriguez-Duarte, N. Joachimowicz, B. Duchêne, E. Tedeschi, M. R. Casu, L. Crocco, and F. Vipiana, "A prototype microwave system for 3d brain stroke imaging," *Sensors*, vol. 20, no. 9, 2020.

[17] D. O. Rodriguez-Duarte, J. A. T. Vasquez, R. Scapaticci, L. Crocco, and F. Vipiana, "Brick-shaped antenna module for microwave brain imaging systems," *IEEE Antennas and Wireless Propagation Letters*, vol. 19, no. 12, pp. 2057–2061, 2020.

[18] Keysight Technologies, "Keysight streamline series USB vector network analyzer P937XA 2-port, up to 26.5 GHz," *Data Sheet*, Oct. 2018.

[19] J. A. Tobon Vasquez, R. Scapaticci, G. Turvani, G. Bellizzi, N. Joachimowicz, B. Duchêne, E. Tedeschi, M. R. Casu, L. Crocco, and F. Vipiana, "Design and experimental assessment of a 2d microwave imaging system for brain stroke monitoring," *International Journal of Antennas and Propagation*, vol. 2019, p. 8065036, May 2019.

[20] D. O. Rodriguez-Duarte, J. A. Tobon Vasquez, R. Scapaticci, L. Crocco, and F. Vipiana, "Assessing a microwave imaging system for brain stroke monitoring via high fidelity numerical modelling," *IEEE Journal of Electromagnetics, RF and Microwaves in Medicine and Biology*, vol. 5, pp. 238–245, Sept. 2021.

[21] N. K. Nikolova, *Introduction to Microwave Imaging*. EuMA High Frequency Technologies Series, Cambridge University Press, 2017.

[22] W.-K. Park, "Application of music algorithm in real-world microwave imaging of unknown anomalies from scattering matrix," *Mechanical Systems and Signal Processing*, vol. 153, p. 107501, 2021.

[23] T. Valeria, A. Ferrero, and M. Sayed, *Modern RF and Microwave Measurement Techniques*. The Cambridge RF and Microwave Engineering Series, Cambridge University Press, 2013.

[24] N. Joachimowicz, B. Duchêne, C. Conessa, and O. Meyer, "Anthropomorphic breast and head phantoms for microwave imaging," *Diagnostics*, vol. 8, no. 4, 2018.

[25] J. Fridriksson, O. Kjartansson, P. S. Morgan, H. Hjaltason, S. Magnusdottir, L. Bonilha, and C. Rorden, "Impaired speech repetition and left parietal lobe damage," *The Journal of neuroscience : the official journal of the Society for Neuroscience*, vol. 30, pp. 11057–11061, Aug 2010.